Ultra-Low Clouds over the Southern West African Monsoon Region

Note: This is the accepted version of the article. Some editorial changes may have been made before publication in GRL. This PDF also contains the auxiliary material. The correct citation is:

Knippertz P., A. H. Fink, R. Schuster, J. Trentmann, and C. Yorke, 2011: Ultra-Low Clouds over the Southern West African Monsoon Region. Geophys. Res. Lett., 38, L21808, doi:10.1029/2011GL049278.

Peter Knippertz

School of Earth & Environment, University of Leeds, Leeds LS2 9JT, UK

Andreas H. Fink, Robert Schuster

Institute for Geophysics and Meteorology, University of Cologne, Kerpener Str. 13, 50923 Köln, Germany

Jörg Trentmann

Satellite Application Facility on Climate Monitoring, German Weather Service, Frankfurter Straße 135, 63067 Offenbach, Germany

Jon M. Schrage

Department of Atmospheric Sciences, Creighton University, 2500 California Plaza, Omaha, NE 68178, USA

Charles Yorke

Ghana Meteorological Agency, P.O. Box LE 87, Legon, Accra, Ghana

Corresponding author: Peter Knippertz (p.knippertz@leeds.ac.uk)

Abstract

New ground- and space-based observations show that summertime southern West Africa is frequently affected by an extended cover of shallow, non-precipitating clouds only few hundred meters above the ground. These clouds are associated with nocturnal low-level wind speed maxima and frequently persist into the day, considerably reducing surface solar radiation. While the involved phenomena are well represented in re-analysis data, climate models show large errors in low-level wind, cloudiness, and solar radiation of up to 90 W m^{-2}. Errors of such a magnitude could strongly affect the regional energy and moisture budgets, which might help to explain the notorious difficulties of many models to simulate the West African climate. More effort is needed in the future to improve the monitoring, modeling, and physical understanding of these ultra-low clouds and their importance for the West African monsoon system.

1. Background

The West African monsoon (WAM) system involves multi-scale interactions between the atmosphere, the ocean, and the land surface. WAM variations affect remote regions such as the North Atlantic, Europe, India, and the tropical Pacific [*Cassou et al.,* 2005*; Losada et al.*, 2010; *Rodríguez-Fonseca et al.,* 2010*; Gaetani et al.*, 2011]. Climate models show large latitudinal biases of the main rain belt [*Cook and Vizy*, 2006] and disagree about the sign of precipitation change for the 21st century [*Christensen et al.,* 2007*; Druyan*, 2010; *Paeth et al.,* 2011]. This uncertainty hinders the development of adaptation strategies for one of the most vulnerable regions worldwide [*Boko et al.,* 2007]. Recent observational, diagnostic, and modeling work has concentrated on the spatio-temporal variability and

47 dynamics of rainfalls over the Sahel, and on external drivers such as sea-surface
48 temperatures, land surface processes, and aerosols [*Lafore et al.*, 2010; *Xue and Ruti*,
49 2010]. Here we use new ground- and space-based observations to show that the frequent
50 occurrence of extended, shallow, ultra-low, non-precipitating stratiform clouds, which form
51 in association with nocturnal low-level wind speed maxima, considerably reduce surface
52 solar radiation over summertime southern West Africa. These clouds have so far received
53 little attention [*Schrage et al.*, 2006; *Schrage and Fink*, 2010] in contrast to their oceanic
54 counterparts [*Albrecht et al.*, 1995] and their role for the whole WAM system is unknown.
55

56 **2. Data**

57 To monitor low-level cloudiness, wind speed, and solar radiation over West Africa a wide
58 range of space- and surface based observations have been used. The former include false-
59 color composites from three infrared (IR) channels from Meteosat Second Generation
60 (MSG), lidar backscatter coefficients from CALIPSO (Cloud-Aerosol Lidar and Infrared
61 Pathfinder Satellite Observations; http://eosweb.larc.nasa.gov/PRODOCS/calipso/
62 table_calipso.html) and radar reflectivity from CloudSat (http://cloudsat.cira.colostate.edu/)
63 [*Stephens et al.*, 2002]. In addition, more derived products such as surface solar irradiance
64 from the Global Energy and Water Cycle Experiment Surface Radiation Budget (GEWEX-
65 SRB) Project [*Stackhouse et al.*, 2011] and low-level cloud cover from the widely used
66 International Satellite Cloud Climatology Project (ISCCP; see http://isccp.giss.nasa.gov)
67 dataset [*Rossow and Schiffer*, 1999] were used. The three-hourly (monthly) ISCCP D1 (D2)
68 product provides fractional cloud cover for levels below 800 hPa (680 hPa). Ground-based

measurements include standard surface SYNOPs and METARs (in particular from Kumasi, Ghana) [*WMO,* 1995], pyranometer measurements of surface solar irradiance at Ilorin (Nigeria), Cotonou, Parakou (both Benin), and Kumasi (Ghana) as well as measurements with an ultra-high frequency profiler [*Lothon et al.*, 2008] and a ceilometer [*Pospichal and Crewell*, 2007] at Djougou (central Benin) deployed during the African Monsoon Multidisciplinary Analysis (AMMA) field campaign in 2006. Wind profiles are taken from 3-hourly radiosondes launched during AMMA, when several new stations were established, allowing for the first time a reliable estimate of the diurnal cycle at the regional scale [*Parker et al.*, 2008]. Here we use all available data from the four stations Abuja (Nigeria), Cotonou, Parakou (both Benin), and Tamale (Ghana).

As a near-observational modeling reference, short-term forecasts started at 0000 UTC every day made in the production of the European Centre for Medium-Range Weather Forecasts (ECMWF) ERA Interim re-analyses [*Dee et al.*, 2011] covering the period 1989–2010 were used on standard pressure levels with a horizontal resolution of 0.5°. The advantages of using short-term forecasts are (i) a 3-hourly time resolution (in contrast to 6-hourly for the actual re-analysis data) and (ii) a physically consistent diurnal cycle using the model forecast times +3h to +24h. Since solar irradiance data are not assimilated, differences between short-term model forecasts and the actual re-analysis are small (not shown). To assess state-of-the-art climate models the World Climate Research Programme's (WCRP's) Coupled Model Intercomparison Project phase 3 (CMIP3) multi-model dataset [*Meehl et al.*, 2007] was used. The analysis concentrates on the period 1961–1999 from the “climate of the 20th Century experiments (20C3M)”, which were initialized in the pre-industrial

control runs. More details on the data used in this paper including a map with all station locations are provided in the Auxiliary Material. All analyses concentrate on the time of the peak summer monsoon July–September and on the geographical region 6–10°N, 7°W–7°E (see black boxes in Figures 2–4).

3. An Example

Figure 1 provides an example of a night with a clear view on an extended cover of low-level stratus over southern West Africa and demonstrates the challenge to observe these with the existing network. MSG IR composites and corresponding human-eye observations agree well on the extent of the cloud deck (Figure 1a). The ISCCP retrieval, however, reveals a dramatic underestimation, mostly likely caused by the small IR contrast to the surface (Figure 1b). A vertical cross section from the CALIPSO lidar (Figure 1c) clearly shows low clouds over southern Nigeria, which are obscured by ground clutter in a corresponding CloudSat radar profile (Figure 1d). Before the new capabilities of MSG and CALIPSO nocturnal low-level clouds were mainly observed by eye from the ground. This is still true today in the presence of elevated layers of cloud and/or aerosol. Measurements with a ceilometer at Djougou (Benin) reveal the extremely low base of the cloud deck over this location, which descends to the surface in the course of the night and then rises and breaks open around noon (Figure 1e). Collocated wind measurements (Figure 1f) show a prominent nighttime maximum in the monsoonal southerlies, often referred to as a nocturnal low-level jet (NLLJ) [*Parker et al.*, 2005; *Lothon et al.*, 2008]. This suggests that shear-induced turbulence below the jet core mixes moist air from the surface upward to create the cloud deck [*Bonner and Winninghoff*, 1969].

4. Observational Climatologies

Recently available longer-term climatologies of clouds and winds confirm these ideas. The summer mean diurnal cycle of low-cloud cover from Kumasi airport (Ghana; Figure 2a) reveals a distinct diurnal cycle with a sharp increase shortly after sunset, a maximum around 75% at sunrise, a slow decrease until the early afternoon, followed by a steep drop below 30% at 2000 UTC. A decrease in cloudiness between morning and early afternoon is also seen in the visible channel of the Moderate Resolution Imaging Spectroradiometer MODIS [*Douglas et al.*, 2010]. ISCCP data largely underestimate low-level cloudiness across large parts of southern West Africa (Figure 2b) and show a reversal of the diurnal cycle (Figure 2a, see also Auxiliary Figure S3). Averaged wind profiles from four radiosondes stations clearly show the NLLJ with maximum wind speeds of ~7 m s^{-1} at 0300 and 0600 UTC and weaker winds during the afternoon (Figure 2c). A second peak of about 8 m s^{-1} is observed at about 680 hPa, possibly to do with the southern flank of the midlevel African Easterly Jet (AEJ). The close correspondence between the diurnal cycles of wind and clouds support the idea of NLLJ-induced mixing of moisture. The persistence of the clouds after sunrise, together with large albedo differences to the underlying lush vegetation (0.9 vs. 0.15), substantially reduces surface incoming solar radiation. Ground observations show summer means as low as 147 W m^{-2} with values increasing towards the Sahel (Figure 2d). The high value of 198 W m^{-2} at Cotonou is most likely only representative of a narrow coastal strip, where the passage of the sea-breeze front in the morning and upwelling of cooler waters along parts of the coastline support clearer skies.

GEWEX satellite retrievals (Figure 2d) show a broad local minimum over southern West Africa with an average of 178.5 W m^{-2} over the box marked in black in Figure 2d (which represents the mostly flat areas away from the Guinean Highlands, the Jos Plateau, and the Cameroon Mountains, see Figure S1 in the Auxiliary Material). The ground observations suggest a slight positive bias in the GEWEX data, potentially related to cloud-detection problems in the morning and evening hours. Other satellite retrievals have larger positive biases (Auxiliary Table S1 and Figures S5 and S6).

Horizontal distributions of low-level cloudiness from the ECMWF ERA-Interim re-analysis (Figure 3a) show a clear maximum over the whole of southern West Africa with particularly high values over orographic features. The regional average of 59% and its diurnal cycle are in good agreement with the observations at Kumasi (Figures 2a and 3a). Vertical profiles of model layer cloud cover (Figure 3b) confirm the gradual spreading of low stratus clouds in the course of the night. After sunrise, the peak in cloudiness broadens vertically and rises to 800 hPa until 1500 UTC. Smallest cloud covers are found at 1800 and 2100 UTC. Above 700 hPa, cloudiness shows a negligible diurnal cycle with a mean cover < 10%. Vertical profiles of wind speed (Figure 3c) also show a strong diurnal cycle in good agreement with radiosonde data (Figure 2c). The slightly weaker mean 925 hPa wind speed of 5.3 m s^{-1} in ERA-Interim compared to 5.8 m s^{-1} in the radiosonde data is most likely due to the coastal station Cotonou with its unrepresentatively high wind speeds (Auxiliary Figure S4). The midlevel maximum is slightly higher in ERA-Interim, possibly due to few stations close to the AEJ core in the north of the region. Solar irradiance

156 estimates (Figure 3d) show a close correspondence to the low cloud cover (Figure 3a) and a
157 good agreement with the station observations with a regional average of 161.3 W m^{-2}.
158
159
160
161 **5. Climate Models**
162 Long-term mean profiles from the CMIP3 multi-model dataset show a general
163 underestimation of low-level clouds and an overestimation of mid-level clouds (Figure 4a)
164 with respect to ERA-Interim. The diversity between models is immense in both cloud
165 amounts and vertical distribution with few showing profiles similar to the re-analysis. Daily
166 mean wind profiles also show considerable variations with many models overestimating
167 NLLJs by almost a factor of 2 with respect to observations (Figure 4b). The problems of
168 representing low (and also midlevel) clouds evident from Figure 4a lead to a massive
169 overestimation of surface solar irradiance over southern West Africa (Figure 4c). The
170 regional average of 190.2 W m^{-2} is almost 30 W m^{-2} larger than that of ERA-Interim with
171 individual models deviating by as much as 98 W m^{-2} (Auxiliary Table S2). All ERA-
172 Interim–CMIP3 model differences are statistically significant on at least the 95% level.
173 Pertinent inter-model standard deviations indicate a maximum disagreement over southern
174 West Africa, particularly over high terrain and the west coast (Figure 4d), with a regional
175 average of 39.4 W m^{-2}. This bias and uncertainty in solar energy input can be expected to
176 influence the surface energy budget, low-level temperature, and pressure, and possibly the

entire monsoon circulation [*Eltahir and Gong*, 1996]. Future research should investigate to what extent these deficits influence the overall model performance for the WAM. Differences between individual models are one order of magnitude larger than typical differences between simulations with or without ocean coupling, and between current and future climates of the same model (Auxiliary Figure S7), making reliable climate-change projections practically impossible.

6. Discussion and Conclusions

Recently available ground- and space-based observations and short-term ECMWF forecasts have been analyzed to better document and understand the climatology of low-level cloudiness over summertime West Africa. Based on this the following mechanism is suggested [see also *Bonner and Winninghoff*, 1969; *Schrage et al.*, 2006; *Schrage and Fink*, 2010]: (I) Around sunset, mixing in the planetary boundary layer breaks down followed by a minimum in cloudiness. (II) Radiative cooling stabilizes a shallow surface layer, where winds slacken and moisture accumulates through evapotranspiration. (III) Due to decoupling from surface friction winds accelerate above the weak surface inversion (few hundred meters above ground) in response to the monsoonal north–south pressure gradient, forming a NLLJ. (IV) Increasing vertical wind shear below the jet mechanically generates turbulence, which mixes moist surface air upwards and leads to the formation of ultra-low clouds. (V) Some nights show several mixing cycles with intermittent turbulence until increased downwelling longwave radiation from the thickened cloud deck stops further cooling of the surface. This creates a positive feedback leading to the predominance of fully overcast nights over southern West Africa during summer (Auxiliary Figure S2). (VI) It can

take until the early afternoon for solar heating to fully erode the NLLJ and cloud deck, which is then often replaced by fair-weather cumuli.

While observations and ECMWF data show an overall satisfactory agreement, CMIP3 climate models tend to show too strong winds and too little cloud cover at low levels. A possible explanation for these biases is too little vertical mixing in the stable nighttime boundary layer, leading to too much decoupling from the surface and thus a reduced upward transport of surface moisture and a too weak deceleration the NLLJ through surface friction. The formation of fog in some models in Figure 4a (e.g. cccma) supports this hypothesis. It is conceivable that the atmospheric moisture budget, especially moisture recycling from vegetation and the low-level northward transport, is also adversely affected by these biases. A possible reason could be insufficient temporal and vertical resolution. The former might cause models to miss out on the first onset of stratus leading to too much radiative cooling and decoupling through positive feedbacks [*Schrage et al.*, 2006]. The latter might not allow models to represent the downward propagation of shear-induced turbulence from underneath the NLLJ core to the surface [*Bain et al.*, 2010]. A comparison between the high- and medium-resolution version of the Miroc3 model (56 vs. 20 levels), however, shows similar overestimations of the NLLJ, but more realistic clouds at high resolution, indicating that other factors must play a role, too. Potentially important are feedbacks of the cloud evolution with the surface energy budget and hydrology, which influences relative humidity and stability. In the real atmosphere, subtle variations in low-level static stability and humidity, as well as in the background pressure gradient that drives the NLLJ, can decide between cloudy and clear nights [*Schrage et al.*, 2006; *Schrage and*

Fink, 2010]. Disentangling the details of the relationship between errors in the large-scale pressure and moisture distributions, clouds, winds, surface hydrology, and radiation in CMIP3 data is beyond the scope of this paper. However, the good representation of all features in the more constraint ECMWF model is encouraging and could serve as a benchmark to evaluate free-running climate models more rigorously, using output with higher temporal resolution to resolve the diurnal cycle and to conduct targeted sensitivity experiments. In parallel, more efforts are needed to improve the representation of low clouds in satellite retrievals for a better observational constraint on models. These, together with ground-based observations from AMMA and other initiatives, will help to build a more robust climatology and to advance our physical understanding of the controls of cloud formation. In the long run, it is hoped that this work will enhance our capability to model the WAM and make better projections of climate change over this crucial region.

Acknowledgments

We acknowledge funding from the German Science Foundation (KN 581/2-3) and for IMPETUS (BMBF Grant 01LW06001A, North Rhine-Westphalia Grant 313-21200200) and QWeCI (EU Grant 243964). The MSG, ceilometer, and wind profiler data (Figure 1) were obtained from the AMMA database and we acknowledge Bernhard Pospichal and Bernard Campistron, respectively. We thank the Kwame Nkrumah University of Science and Technology for supporting the Kumasi field site, the World Radiation Monitoring Center for radiation data from Ilorin, the NASA CloudSat project for CloudSat data, and the UK Met Office for providing access to ERA-Interim re-analyses. The GEWEX SRB and CALIPSO data were obtained from the NASA Langley Research Center Atmospheric

244 Sciences Data Center. We acknowledge the modeling groups, the Program for Climate
245 Model Diagnosis and Intercomparison, and the WCRP's Working Group on Coupled
246 Modelling for their roles in making available the WCRP CMIP3 multi-model
247 dataset, support of which is provided by the Office of Science, U.S. Department of Energy.
248 We would also like to thank two anonymous reviewers for their helpful comments.

249 **References**

250 Albrecht, B. A., C. S. Bretherton, D. Johnson, W. H. Schubert, and A. S. Frisch (1995), The
251 Atlantic Stratocumulus Transition Experiment – ASTEX, *Bull. Am. Meteorol. Soc., 76,*
252 889–904.

253 Bain, C. L., D. J. Parker, C. M. Taylor, L. Kergoat, and F. Guichard (2010), Observations
254 of the nocturnal boundary layer associated with the West African Monsoon, *Mon. Wea.*
255 *Rev., 138,* 3142–3156.

256 Boko, M., et al. (2007), Africa, in *Climate Change 2007: Impacts, adaptation and*
257 *vulnerability. Contribution of Working Group II to the Fourth Assessment Report of the*
258 *Intergovernmental Panel on Climate Chang*, edited by M. L. Parry, et al., pp. 433–467,
259 Cambridge University Press, Cambridge, UK.

260 Bonner, W. D., and F. Winninghoff (1969), Satellite studies of clouds and cloud bands near
261 the low-level jet, *Mon. Wea. Rev., 97,* 490–500.

262 Cassou, C., L. Terray, and A. S. Phillips (2005), Tropical Atlantic influence on European
263 heatwaves, *J. Clim., 18,* 2805–2811.

264 Christensen, J. H., et al. (2007), Regional climate projections, in *Climate Change 2007:*
265 *The physical science basis. Contribution of Working Group I to the Fourth Assessment*

Report of the Intergovernmental Panel on Climate Change, edited by S. Solomon, et al., pp. 847–940, Cambridge University Press, Cambridge, UK and New York, NY, USA.

Cook, K. H., and E. K. Vizy (2006), Coupled model simulations of the West African monsoon system: 20th century simulations and 21st century predictions, *J. Clim., 19*, 3681–3703.

Dee, D. P., et al. (2011), The ERA-Interim reanalysis: configuration and performance of the data assimilation system, *Q. J. R. Meteorol. Soc., 137*, 553–597.

Douglas, M., R. Beida, and A. Dominguez (2010), Developing high spatial resolution daytime cloud climatologies for Africa, paper presented at 29th Conference on Hurricanes and Tropical Meteorology, Tucson, AZ.

Druyan, L. M. (2010), Studies of 21st-century precipitation trends over West Africa, *Internat. J. Climatol.,* doi:10.1002/joc.2180.

Eltahir, E. A. B., and C. Gong (1996), Dynamics of the wet and dry years in West Africa, *J. Clim., 9*, 1030–1042.

Gaetani, M., B. Pohl, H. Douville, and B. Fontaine (2011), West African Monsoon influence on the summer Euro-Atlantic circulation, *Geophys. Res. Lett., 38*, L09705.

Lafore, J.-P., C. Flamant, V. Giraud, F. Guichard, P. Knippertz, J.-F. Mahfouf, P. Mascart, and E. R. Williams (2010), Introduction to the AMMA Special Issue on 'Advances in understanding atmospheric processes over West Africa through the AMMA field campaign, *Q. J. R. Meteorol. Soc., 136*, 2–7.

Losada, T., B. Rodríguez-Fonseca, I. Polo, S. Janicot, S. Gervois, F. Chauvin, and P. Ruti (2010), Tropical response to the equatorial mode: AGCM multimodel approach, *Clim. Dyn., 35*, 45–52.

289 Lothon, M., F. Saïd, F. Lohou, and B. Campistron (2008), Observation of the diurnal cycle
290 in the low troposphere of West Africa, *Mon. Wea. Rev., 136,* 3477–3500.
291 Meehl, G. A., C. Covey, T. Delworth, M. Latif, B. McAvaney, J. F. B. Mitchell, R. J.
292 Stouffer, and K. E. Taylor (2007), The WCRP CMIP3 multi-model dataset: A new era in
293 climate change research, *Bull. Am. Meteorol. Soc., 88,* 1383–1394.
294 Paeth, H., et al. (2011), Progress in regional downscaling of West African precipitation,
295 *Atmos. Sci. Lett.,* 12, 75–82.
296 Parker, D. J., R. R. Burton, A. Diongue-Niang, R. J. Ellis, M. Felton, C. M. Taylor, C. D.
297 Thorncroft, P. Bessemoulin, and A. M. Tompkins (2005), The diurnal cycle of the West
298 African monsoon circulation, *Q. J. R. Meteorol. Soc.,* 131, 2839–2860.
299 Parker, D. J., et al. (2008), The AMMA radiosonde program and its implications for the
300 future of atmospheric monitoring over Africa, *Bull. Am. Meteorol. Soc., 89,* 1015–1027.
301 Pospichal, B., and S. Crewell (2007), Boundary layer observations in West Africa using a
302 novel microwave radiometer, *Meteorol. Z., 16(5),* 513–523.
303 Rodríguez-Fonseca, B., I. Polo, J. Garcia-Serrano, T. Losada, E. Mohino, C. R. Mechoso,
304 and F. Kucharski (2009), Are Atlantic Niños enhancing Pacific ENSO events in recent
305 decades?, *Geophys. Res. Lett., 36,* L20705, doi:10.1029/2009GL040048.
306 Rossow, W. B., and R. A. Schiffer (1999), Advances in understanding clouds from ISCCP,
307 *Bull. Am. Meteorol. Soc., 80,* 2261–2288.
308 Schrage, J. M., S. Augustyn, and A. H. Fink (2006), Nocturnal Stratiform Cloudiness
309 during the West African Monsoon, *Meteorol. Atmos. Phys., 95,* 73–86.

Schrage, J. M., and A. H. Fink (2010), A possible mechanism regulating nocturnal stratocumulus decks in West Africa, paper presented at 29th Conference on Hurricanes and Tropical Meteorology, Tucson, AZ.

Stackhouse Jr., P. W., S. K. Gupta, S. J. Cox, T. Zhang, J. C. Mikovitz, and L. M. Hinkelman (2011), 24.5-year SRB data set released, *GEWEX News, 21(1),* 10–12.

Stephens, G., et al. (2002), The Cloudsat mission and the A-train, *Bull. Am. Meteorol. Soc.*, *83,* 1771–1790.

World Meteorological Organization (1995), *Manual on codes. International Codes, Vol. I.1, Part A—Alphanumeric Codes*. WMO-No. 306, World Meteorological Organization, Geneva, Switzerland.

Xue, Y., and P. M. Ruti, (2010), Prelude to Special Issue: West African monsoon and its modeling, *Clim. Dyn., 35,* 1–2.

Figure Captions

Figure 1. Example case 20 August 2006. (a) MSG IR composite at 0130 UTC on (low clouds in green) with 0300 UTC ground observations of low-cloud cover in octas as symbols. (b) ISCCP 3-hourly mean low-cloud cover centered on 0000 UTC. (c) and (d) Vertical profiles at 0130 UTC and orography along the track shown in (A) from the CALIPSO lidar and CloudSat radar. (e) and (f) 1600 UTC 19 – 1600 UTC 20 August observations of clouds and winds from a ceilometer and a ultra-high frequency profiler at Djougou (central Benin).

Figure 2. Summer climatologies from observations. (a) Mean diurnal cycle of low-cloud cover from eye observations at Kumasi airport (Ghana; 2010 only), and regional averages from ERA-Interim (1989–2010, see Figure 3) and ISCCP D2 (1983–2007). (b) Corresponding horizontal distribution from ISCCP D2 with the 60% observations from Kumasi marked, both averaged over the diurnal cycle and the same years as in (a). (c) Mean diurnal cycle of vertical profiles of wind speed from the radiosonde stations Abuja, Cotonou, Parakou, and Tamale during 2006 (mean in blue). (d) Solar irradiance at the surface from GEWEX satellite data 1983–2007 and the four ground stations Ilorin, Cotonou, Parakou, and Kumasi as numbers (observation periods are given in the Auxiliary Material). All means are calculated from available July–September observations. Black boxes mark the area used for spatial averaging (6–10°N, 7°W–7°E).

Figure 3. Summer climatologies from ERA-Interim re-analysis short-term forecasts. (a) Daily mean low-level cloud cover [%]. (b) and (c) Regionally averaged diurnal cycles of vertical profiles of layer cloud cover and wind speed, respectively (means in black). (d) Solar irradiance at the surface. All means are calculated from July–September 1989–2010. Black boxes and observations from ground stations are as in Figure 2.

Figure 4. Summer climatologies from the CMIP3 multi-model dataset. (a) and (b) Regionally averaged daily mean vertical profiles of layer cloud cover (16 models; ERA-Interim mean in black) and wind speed (20 models with mean dashed; solid black line is calculated from daily averages of the zonal and meridional wind component from ERA-Interim data; models with asterisk have monthly data only). (c) Mean and (d) standard

353 deviation of solar irradiance at the surface (19 models). All CMIP3 model values are
354 calculated from July–September 1961–1999. Black boxes are as in Figures 2 and 3.

Figures

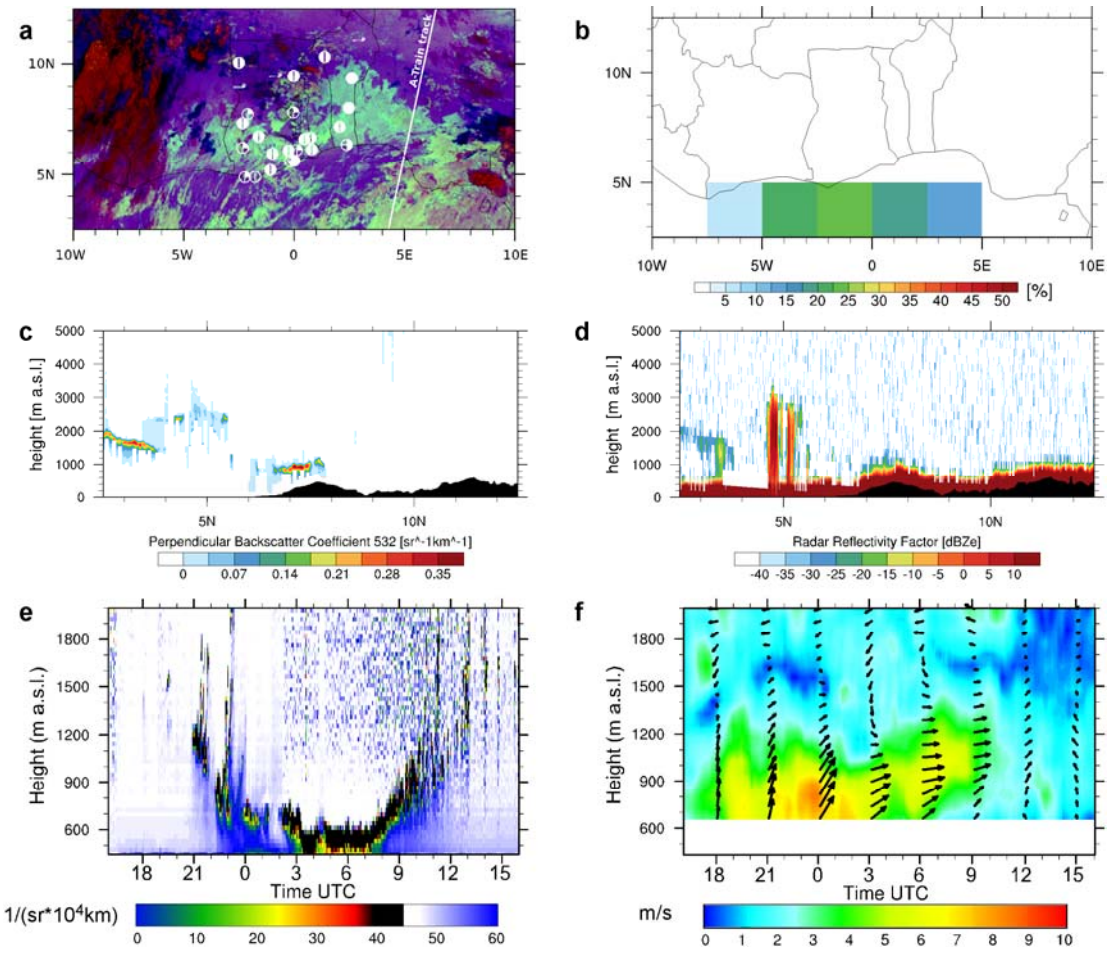

Figure 1. Example case 20 August 2006. (a) MSG IR composite at 0130 UTC on (low clouds in green) with 0300 UTC ground observations of low-cloud cover in octas as symbols. (b) ISCCP 3-hourly mean low-cloud cover centered on 0000 UTC. (c) and (d) Vertical profiles at 0130 UTC and orography along the track shown in (A) from the CALIPSO lidar and CloudSat radar. (e) and (f) 1600 UTC 19 – 1600 UTC 20 August observations of clouds and winds from a ceilometer and a ultra-high frequency profiler at Djougou (central Benin).

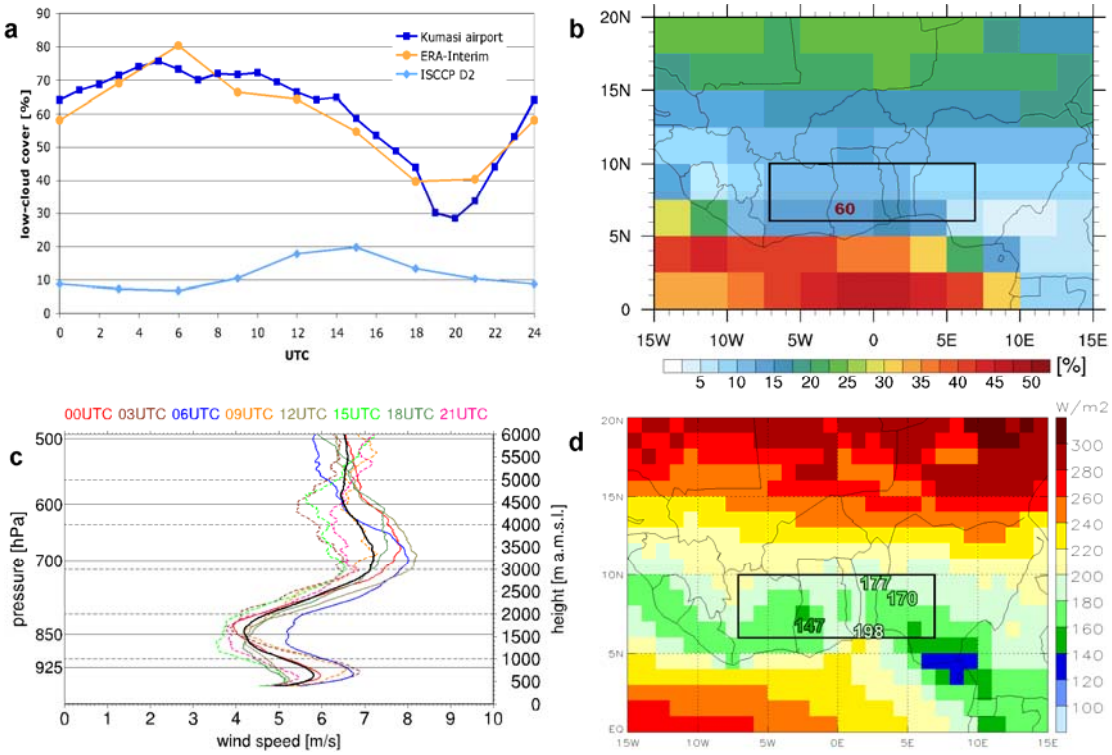

Figure 2. Summer climatologies from observations. (a) Mean diurnal cycle of low-cloud cover from eye observations at Kumasi airport (Ghana; 2010 only), and regional averages from ERA-Interim (1989–2010, see Figure 3) and ISCCP D2 (1983–2007). (b) Corresponding horizontal distribution from ISCCP D2 with the 60% observations from Kumasi marked, both averaged over the diurnal cycle and the same years as in (a). (c) Mean diurnal cycle of vertical profiles of wind speed from the radiosonde stations Abuja, Cotonou, Parakou, and Tamale during 2006 (mean in blue). (d) Solar irradiance at the surface from GEWEX satellite data 1983–2007 and the four ground stations Ilorin, Cotonou, Parakou, and Kumasi as numbers (observation periods are given in the Auxiliary Material). All means are calculated from available July–September observations. Black boxes mark the area used for spatial averaging (6–10°N, 7°W–7°E).

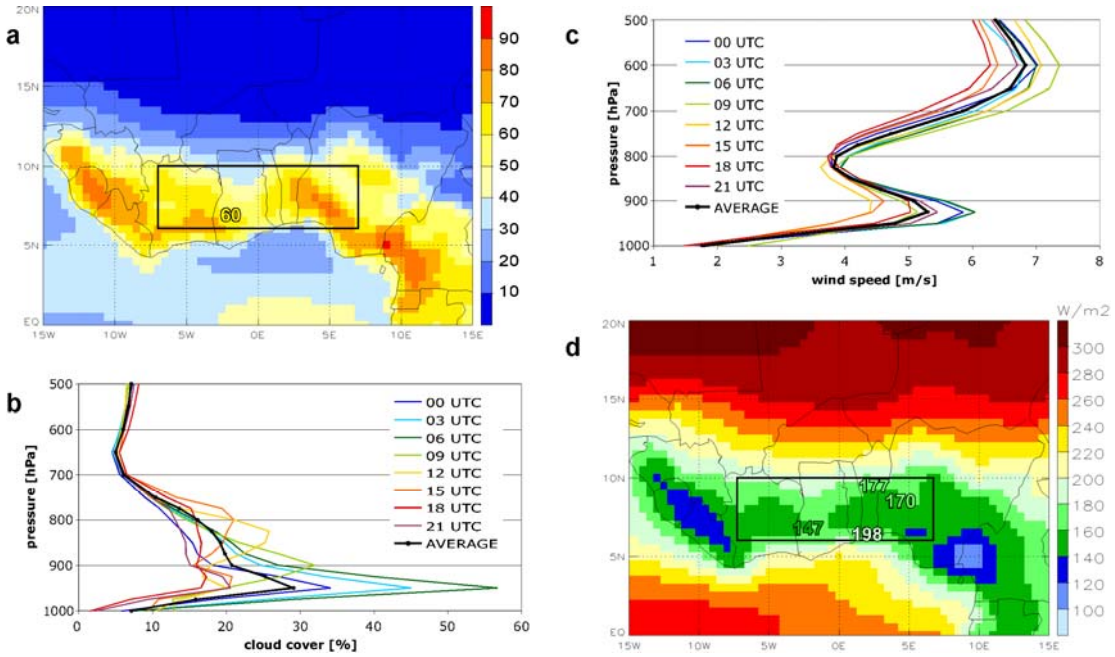

Figure 3. Summer climatologies from ERA-Interim re-analysis short-term forecasts. (a) Daily mean low-level cloud cover [%]. (b) and (c) Regionally averaged diurnal cycles of vertical profiles of layer cloud cover and wind speed, respectively (means in black). (d) Solar irradiance at the surface. All means are calculated from July–September 1989–2010. Black boxes and observations from ground stations are as in Figure 2.

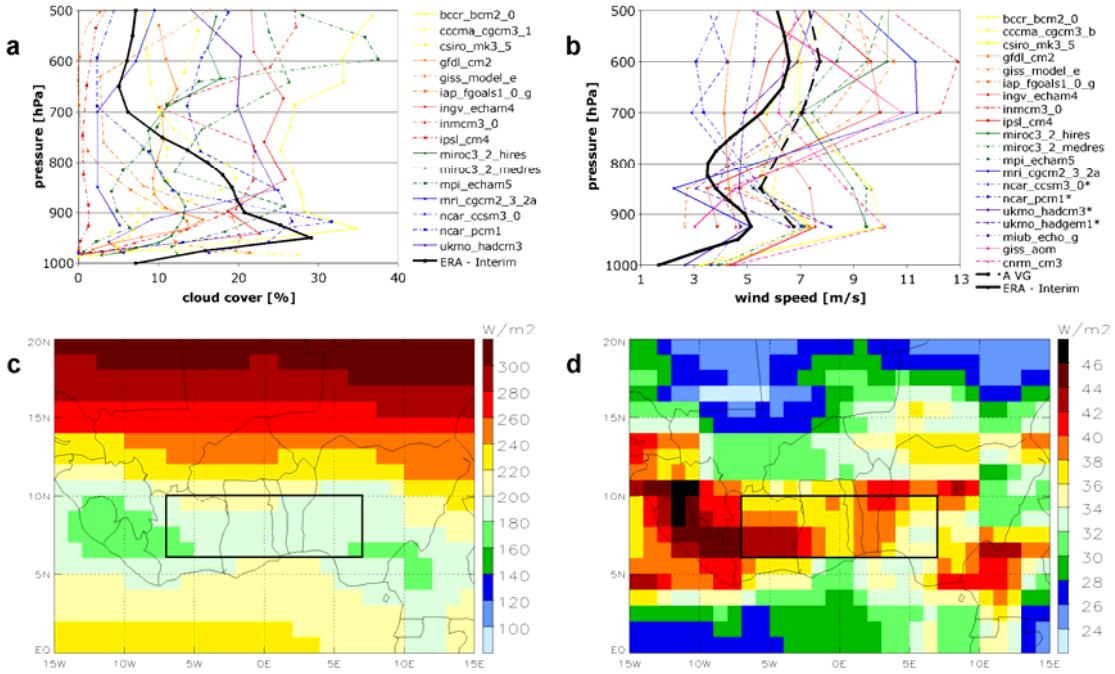

382

383 **Figure 4.** Summer climatologies from the CMIP3 multi-model dataset. (a) and (b)
384 Regionally averaged daily mean vertical profiles of layer cloud cover (16 models; ERA-
385 Interim mean in black) and wind speed (20 models with mean dashed; solid black line is
386 calculated from daily averages of the zonal and meridional wind component from ERA-
387 Interim data; models with asterisk have monthly data only). (c) Mean and (d) standard
388 deviation of solar irradiance at the surface (19 models). All CMIP3 model values are
389 calculated from July–September 1961–1999. Black boxes are as in Figures 2 and 3.